A finite set of content-free pointers in visual working memory: magnetoencephalography (MEG) evidence

Xinchi Yu[a,b] and Ellen Lau[a,b]

Human visual working memory (VWM) is known to be capacity-limited, but the nature of this limit continues to be debated. Recent work has proposed that VWM is supported by a finite (~3) set of content-free pointers, acting as stand-ins for individual objects and binding features together. According to this proposal, the pointers do not represent features within themselves, but rather bind features represented elsewhere together. The current study set out to test if neural hallmarks resembling these content-free pointers can be observed with magnetoencephalography (MEG). Based on two VWM delay-match-to-sample experiments ($N = 20$ each) examining memory for simple and complex objects, we report a sustained response in MEG over right posterior cortex whose magnitude tracks the core hypothesized properties of this content-free pointer system: load-dependent, capacity-limited, and content-free. These results provide novel evidence for a finite set of content-free pointers underlying VWM. *NeuroReport* **36: 153–160**

NeuroReport 2025, **36**:153–160

Keywords: magnetoencephalography (MEG), pointer, right posterior activity, visual short-term memory, visual working memory

[a]Program in Neuroscience and Cognitive Science and [b]Department of Linguistics, University of Maryland, College Park, Maryland, USA

Correspondence to Xinchi Yu, BS, Program in Neuroscience and Cognitive Science, University of Maryland, College Park, MD, USA
E-mail: xcyu@umd.edu

Received 4 December 2024 **Accepted** 9 December 2024.

Introduction

Visual working memory [VWM or visual short-term memory(VSTM)] for objects is a crucial yet extremely capacity-limited faculty for humans [1–7]. Recent work has attempted to reconcile earlier debates between 'object-only' or 'feature-only' theories of the capacity limit with theories of VWM architecture that contain elements of both and are, thus, better able to account for the ever-growing body of experimental findings at the same time (for a review see [8]). One such proposal is that VWM is implemented by a capacity-limited, content-free set of pointers [9–12]: the finite set of pointers (or indexes/indexicals/tokens) act as stand-ins for each individual object in the mind [13–15] and bind features together for the corresponding objects. For example, to represent an individual red square, a pointer would be set up in the mind that binds the RED feature and the SQUARE feature together. This is different from traditional conjunctive coding, where a given neuron might only respond to the combination of RED and SQUARE, because in a conjunctive code, a unit always responds to this particular combination, and in that sense, both red and square are part of its 'content'. In contrast, a content-free pointer has no permanent content, as it can bind different features from moment to moment [16,17]. In this sense, neither the RED feature nor the SQUARE feature is represented within the pointer itself. This model, therefore, has allowed for separate capacity limits for pointers and visual features [9,18–21]. Per theory, the representation for pointers in the brain, if any, needs to meet the following three criteria: (1) load-dependent: that this representation covaries with (within-capacity) VWM load; (2) capacity-limited (i.e. finiteness): that this representation reaches some kind of plateau or homeostasis beyond VWM capacity (of ~3 objects); and (3) content-free: the pointers contain only addresses, not the features themselves, and their function is to bind the addressed features together. The current study looks for such neural responses in magnetoencephalography (MEG). Recent electroencephalography (EEG) evidence supports the existence of content-free representations in VWM with machine-learning multivariate decoding [10] or univariate event-related potentials (ERPs) [14,22,23]; however, it is yet unclear whether these neural markers reflect the capacity limit. Furthermore, earlier functional MRI (fMRI) evidence in fact suggested univariate representations in the brain that meets all three criteria, in regions including the posterior parietal cortex [12,24]. The limitation of fMRI, however, is that it is hard to tell apart perceptual and VWM processes temporally; methods such as EEG and MEG have superior temporal resolution. Here, we offer MEG evidence supporting the existence of VWM pointer representations that meet all three criteria: a right posterior MEG component is load-dependent, capacity-limited (finite), and content-free at the same time.

Previous MEG studies have identified load-dependent, capacity-limited responses during VWM in left and right posterior channels [25–27], but with a bilateral-presentation paradigm and a lateralized change-detection task, with the hope of finding a CDA-like (CDA: contralateral delay activity) response as in EEG. In EEG

DOI: 10.1097/WNR.0000000000002132

studies examining the CDA response, separate stimuli are presented on the left and right sides of the screen, respectively. The participants are cued beforehand to memorize the memorandum on one of the two sides (this being a lateralized as opposed to a whole-field change-detection task [28]). The CDA is computed by subtracting ipsilateral from contralateral ERP responses during the delay between the memorandum and the probe, and its amplitude is load-dependent and capacity-limited with the hope of finding a CDA-like response as in EEG [29,30].. For EEG, posterior responses contralateral to the attended side were found to be modulated by VWM load, while ipsilateral responses are minimally affected by VWM load [31]. Moreover, the attended side of the memorandum accompanies a clear maxima in contralateral posterior electrodes for EEG during the delay between the memorandum and the probe [32]. However, MEG studies have found that the amplitude of responses in both ipsilateral and contralateral posterior channels can be modulated by VWM load [26]. Moreover, side-sensitive channels in MEG appeared to cluster around the midline, rather than being lateralized [27]. Taken together, it is unclear whether posterior responses in MEG reflect the exact same neural sources as for CDA in EEG [26,33]; therefore, a similar lateralized task and contralateral-minus-ipsilateral treatment of data for MEG may not be necessary. In the current study, we employed a similar logic as in the pioneering fMRI study of Xu and Chun [12]. In experiment 1, we tested whether the left and right posterior effects in MEG are still load-dependent and capacity-limited with a central-presentation paradigm and a whole-field change-detection task (as in the study by Xu and Chun [12]). To preview, we found a reliable load-dependent and capacity-limited effect in right posterior channels. In experiment 2, we showed that this right posterior load-dependent, capacity-limited effect is also content-free. Therefore, this right posterior activity (RPA) meets all three criteria for a neural index of VWM pointers.

Methods

Participants

For experiment 1, 20 participants entered data analysis (12 female, age 19–41, M = 24, three left-handed); one additional participant's data was excluded from analysis due to excessive noise (see the Magnetoencephalography analysis section). For experiment 2, 20 participants entered data analysis (13 female, age 18–37, M = 21, two left-handed); one additional participant's data was excluded from analysis due to excessive noise. All subjects reported having normal or corrected-to-normal vision. Informed consent was obtained from all participants and they received monetary reimbursement for their participation. Procedures were approved by the UMD IRB Office.

Procedure

Experiments 1 and 2 had the same procedure. Each subject was presented with two blocks of 200 trials each, which differed in the features of the objects: one block in which the objects were colored squares, and another block in which the objects were complex shapes. The order of the blocks was balanced across subjects. For each block, there were 50 trials for each VWM load condition (1, 2, 4, and 6); within each 50 trials, half of the trials had a match probe and the other half had a change probe.

In each trial, the participants were first presented with a fixation cross with a duration of 500 ms (experiment 1) or 800 ms (experiment 2) against a gray background, followed by a sample screen with a duration of 160 ms (experiment 1) or 200 ms (experiment 2) (because of a programming issue, five participants in experiment 1 had a fixation cross duration of 800 ms, and five participants in experiment 2 had a sample duration of 160 ms). Then, they were presented with the sample; see Fig. 1. The sample consisted of 1, 2, 4, and 6 different objects: for colored square trials, they were sampled from eight colors [black (0,0,0), dark blue (0,0,139), green (0,255,0), light blue (173,216,230), pink (255,192,203), red (255,255,0), white (255,255,255), and yellow (255,255,0)]; for complex shape trials, they were sampled from nine complex shapes similar to those used in the study by Xu and Chun [12]. Eight fixed locations were evenly distributed 4.5° from the center of the screen, and these locations were marked by eight light gray squares (2.5° × 2.5° each). The objects (colored squares or complex shapes) were presented at the center of the light gray squares, spanning 2.1° × 2.1°. The light gray squares served as a visual cue to encourage the individuation of each object and to discourage grouping. A blank screen delay of 1000 ms followed the sample, after which the probe appeared on the screen. At the probe, only one object was presented at one of the eight locations. On 'match' trials, this object was the same one as the one in the sample for that location; on 'change' trials, this probe object was randomly selected from other objects used in this block. Participants pressed one button to indicate 'match', and pressed another button to indicate 'change' (buttons balanced across participants), with no time limit for response. After their response, they were shown a feedback screen for 600 ms, followed by an intertrial interval (ITI) of 2500–3500 ms. During the ITI, a line of asterisks was presented on the screen; before the experiment, participants were instructed to blink only during this period and to avoid blinking during the trials. While the fixation cross was presented on the screen, the participants were instructed to fixate at the center of the screen. They were also instructed against verbal rehearsal. At least eight practice trials for each block were run before the main experiment for each participant, and a self-paced break was administered every 50 trials. Experiment 1 analyses included only the colored

Fig. 1

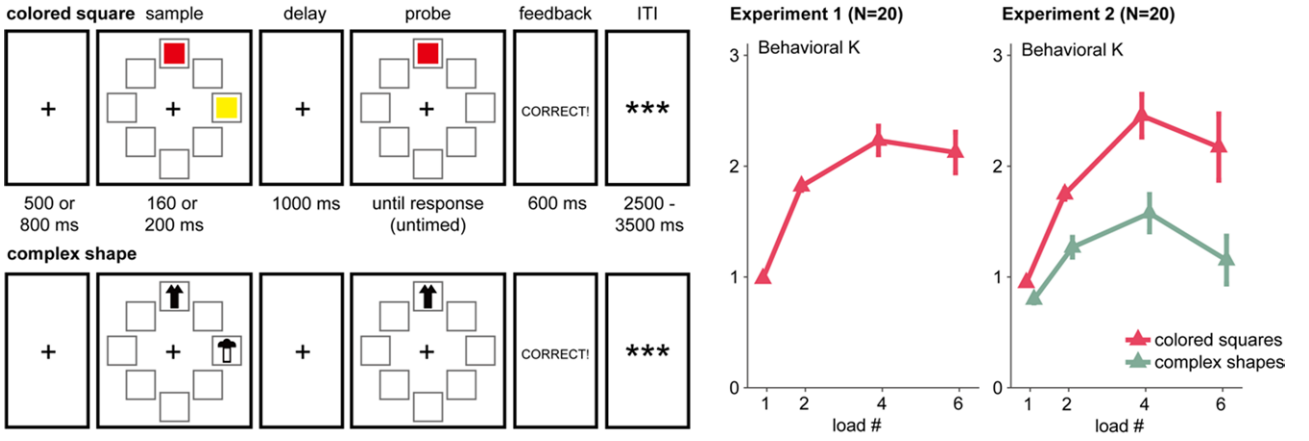

Experimental procedure and behavioral results (Cowan's K) across experiments 1 and 2. Error bars stand for standard error. For detailed presentation parameters of the stimuli, see Procedure. ITI, intertrial interval.

square block (we originally included a complex shape block in experiment 1, but due to a timing error we were unable to analyze the data for those trials), while experiment 2 analyses included both a colored square block and a complex shape block (order balanced across participants). The experiment was run in MATLAB R2009a with Psychtoolbox 3 [34,35].

Behavioral analysis

Based on the hit rates and false alarm rates for each condition, we calculated Cowan's K [1,36], which reflects the number of objects successfully held in VWM. The formula for Cowan's K is as follows: $K = N \times (H - F)$, where N is sample load (i.e. 1, 2, 4, or 6), H is the hit rate for detecting the change in the probe on change trials, and F is the false alarm rate (erroneously 'hallucinating' a change in the probe on match trials).

Magnetoencephalography recording

Before recording, five head position indicator coils were affixed to each participant's head, and the position of these coils relative to the nasion and tragus, as well as the participant's head-shape, was digitized using a Polhemus 3SPACE FASTRAK system to determine the participant's accurate placement in the MEG dewar. During the experimental sessions, participants laid supine in a dimly lit magnetically shielded room (Yokogawa Industries, Tokyo, Japan). Continuous MEG recording was executed using a 160-channel axial gradiometer whole-head system (Kanazawa Institute of Technology, Kanazawa, Japan), and data were sampled at 1000 Hz (60 Hz online notch filter, DC-200 Hz recording bandwidth).

Magnetoencephalography analysis

MEG data were analyzed by customized code in MATLAB R2020b with MNE-Python 1.5.1 [37]. First, noisy and flat channels were identified for each participant with Maxwell filtering, and these channels were interpolated with the MNE algorithm (no channels in the regions of interest (ROIs) described below required interpolation). Then the environmental magnetic interferences were suppressed using temporal signal space separation [38]. A low-pass infinite impulse response (IIR) filter with an upper cutoff frequency of 40 Hz was applied to the MEG data. Ocular and cardiac artifacts were removed using independent component analysis (ICA; fastica algorithm); 2–5 ICA components were removed from each participant. Epochs of –200:1200 ms time-locked to the presentation of sample stimuli in each trial were extracted. The 200 ms prestimulus interval was used as the baseline interval. Trials with a maximum peak-to-peak signal amplitude higher than 3000 fT were excluded. Participants with less than 40 valid trials per condition were excluded from data analysis (one for each experiment, see the Participants section). For the analyzed participants, only 0.7% (experiment 1), 0.1% (experiment 2, colored squares), and 0.4% (experiment 2, complex shapes) of all trials were excluded. For each participant and each condition (i.e. a certain load condition in a certain feature block), we calculated the mean event-related field (ERF) response for each channel.

The first 20 trials in each condition of experiment 1 were used to determine ROIs across both experiments, and as such were excluded from all subsequent analyses. The contrast used for ROI selection was the mean ERF difference between larger (load 4 and 6) vs. smaller (load 1 and 2) conditions (Fig. 2). In line with previous reports [25–27], we observed two opposing maxima in posterior channels. We took three channels each from the two maxima to construct right and left parietal ROIs (right: MEG054, MEG055, and MEG071; left: MEG051, MEG050, and MEG076), and computed mean ERFs for

Fig. 2

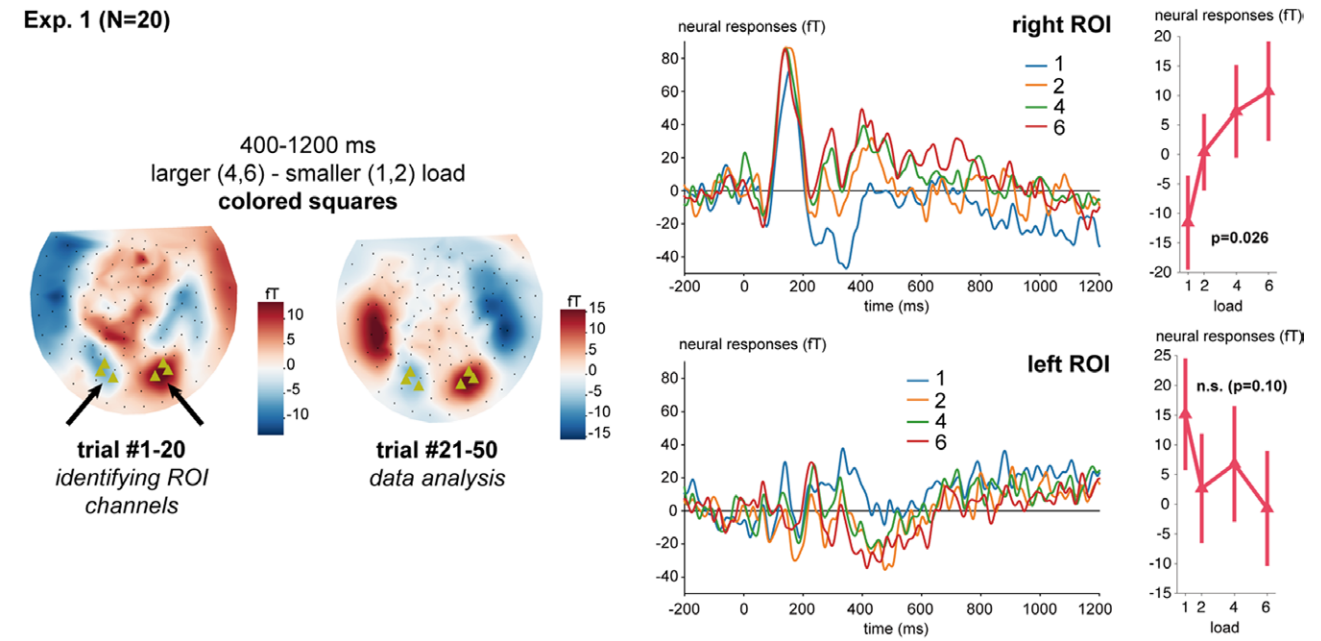

A summary of the MEG results in experiment 1. Error bars stand for standard error. The ROI channels are marked with green triangles. MEG, magnetoencephalography; ROI, region of interest.

each from 400:1200 ms poststimulus-onset to capture the VWM maintenance (as opposed to perception) period.

Comparisons between conditions were statistically evaluated with repeated measures analysis of variance (ANOVA) (using the Greenhouse-Geisser whenever the sphericity assumption was not met), and post hoc comparisons were Bonferroni corrected. In order to better evaluate whether there was a response plateau beyond the capacity limit, we also administered Bayesian repeated-measures ANOVA with a uniform prior, and the post hoc comparisons were administered with Bayesian paired samples *t*-test (with a default Cauchy prior). All statistical analyses reported in this paper were conducted with JASP 0.18.1 [39] and Bayesian factors (BFs) were interpreted following [40]: a BF higher than 10 or lower than 1/10 is considered 'strong', between 3 and 10 or 1/10 and 1/3 is considered 'moderate', and between 1/3 and 3 is considered 'weak'.

Results

Experiment 1

Behavioral results

Repeated measures ANOVA revealed a significant main effect of load, $F(1.80,34.28) = 30.22$, $P < 0.001$. Post hoc comparisons (Bonferroni corrected) revealed a significant difference between loads 1 vs. 2 [$t(19) = -5.75$, $P < 0.001$], 1 vs. 4 [$t(19) = -8.59$, $P < 0.001$], 1 vs. 6 [$t(19) = -7.84$, $P < 0.001$] and 2 vs. 4 [$t(19) = -2.84$, $P = 0.038$]. The difference between 2 vs. 6 [$t(19) = -2.10$, $P = 0.24$] did not reach statistical significance, nor did the difference between 4 vs. 6 [$t(19) = 0.74$, $P = 1$]. Bayesian repeated measures ANOVA revealed strong evidence for the effect of load, $BF_{incl} = 1.66 \times 10^{10}$. There was strong evidence for a difference between 1 vs. 2 ($BF_{10} = 1.09 \times 10^{12}$), 1 vs. 4 ($BF_{10} = 1.73 \times 10^{6}$), 1 vs. 6 ($BF_{10} = 4.13 \times 10^{3}$), and 2 vs. 4 ($BF_{10} = 16.11$), and moderate evidence against a difference between 4 vs. 6 ($BF_{10} = 0.28$), suggesting a plateau of Cowan's K beyond a load of ~4. The evidence for a difference between 2 vs. 6 was weak ($BF_{10} = 0.79$).

Magnetoencephalography results

The repeated measures ANOVA for MEG responses in the right ROI (Fig. 2) showed a statistically significant main effect of load, $F(1.98,37.52) = 4.06$, $P = 0.026$. Post hoc comparisons (Bonferroni corrected) revealed a significant difference between loads 1 vs. 4 [$t(19) = -2.73$, $P = 0.050$] and 1 vs. 6 [$t(19) = -3.23$, $P = 0.012$]. The other comparisons did not reach statistical significance (P's > 0.5). Bayesian repeated measures ANOVA revealed moderate evidence for the effect of load, $BF_{incl} = 4.15$. There was moderate evidence for the difference between 1 vs. 6 ($BF_{10} = 3.71$), as well as moderate evidence against a difference between 4 vs. 6 ($BF_{10} = 0.27$). Evidence for other differences was weak ($1/3 < BF_{10} < 3$). We note that our number of trials per load condition (~30) here is rather low compared with previous MEG studies of this kind ([26]: 384 trials/condition; [27]: 200 trials/condition; and [25]: 120 trials/condition) but with a similar sample size. Below we pool all 40 participants across the two experiments for a higher powered analysis.

In the left ROI, the main effect of the load was not statistically significant, $F(3,57) = 2.15$, $P = 0.10$. Evidence for the effect of load was also weak, $BF_{incl} = 0.62$.

Experiment 2

Behavioral results

A repeated measures ANOVA crossing load and feature (colored square vs. complex shape), showed a significant main effect of load on Cowan's K, [$F(1.51,28.76) = 16.38$, $P < 0.001$], a main effect of feature [$F(1,19) = 50.45$, $P < 0.001$], and a significant interaction [$F(2.13,40.48) = 7.35$, $P = 0.002$]. Bayesian repeated measures ANOVA also revealed strong evidence for the effect of load ($BF_{incl} = 2.42 \times 10^7$), feature ($BF_{incl} = 4.61 \times 10^5$) and the interaction effect ($BF_{incl} = 715.77$). The main effect of feature reflected overall higher performance for colored squares than complex shapes, in line with previous observations, for example, [12].

We followed up the interaction with one-way ANOVAs at each level of feature. In colored square trials, the main effect of load was statistically significant, $F(1.55,29.42) = 18.16$, $P < 0.001$. Post hoc comparisons (Bonferroni corrected) revealed significant differences between loads 1 vs. 2 [$t(19) = -3.67$, $P = 0.003$], 1 vs. 4 [$t(19) = -6.92$, $P < 0.001$], 1 vs. 6 [$t(19) = -5.62$, $P < 0.001$], and 2 vs. 4 [$t(19) = -3.25$, $P = 0.012$]. The differences between 2 vs. 6 [$t(19) = -1.95$, $P = 0.34$] and 4 vs. 6 [$t(19) = 1.30$, $P = 1$] were not statistically significant. Bayesian repeated measures ANOVA also suggested strong evidence for the effect of load, $BF_{incl} = 1.82 \times 10^6$. There was strong evidence for the difference between 1 vs. 2 ($BF_{10} = 1.36 \times 10^{11}$), 1 vs. 4 ($BF_{10} = 1.08 \times 10^5$), 1 vs. 6 ($BF_{10} = 63.91$) and 2 vs. 4 ($BF_{10} = 87.07$). Evidence for the difference between 2 vs. 6 ($BF_{10} = 0.61$) and 4 vs. 6 ($BF_{10} = 0.44$) was weak.

In complex shape trials, the main effect of the load was also significant [$F(1.99,37.74) = 7.01$, $P = 0.003$]. Post hoc comparisons (Bonferroni corrected) revealed significant differences between loads 1 vs. 2 [$t(19) = -2.74$, $P = 0.049$] and 1 vs. 4 [$t(19) = -4.53$, $P < 0.001$]. The other differences were not statistically significant (P's > 0.09). Bayesian repeated measures ANOVA also suggested strong evidence for the effect of load, $BF_{incl} = 93.00$, and for the difference between 1 vs. 2 ($BF_{10} = 6.03 \times 10^4$) and 1 vs. 4 ($BF_{10} = 136.50$). Evidence for the other differences was weak ($1/3 < BF_{10} < 3$).

In sum, the colored square and complex shape comparisons patterned similarly in showing the main effects of load. The interaction between feature and load appeared to be driven only by the slight drop observed in performance for complex shapes at load 6.

Magnetoencephalography results

The 2 × 4 (feature × load) repeated measures ANOVA for MEG responses in the right ROI (Fig. 3) showed a significant main effect of load [$F(1.50,28.47) = 6.31$, $P = 0.010$]. The main effect of feature [$F(1,19) = 0.086$, $P = 0.77$] and the interaction effect [$F(3,57) = 0.90$, $P = 0.45$] were NS. Post hoc comparisons between load conditions (Bonferroni corrected) revealed a significant difference between loads 1 vs. 4 [$t(19) = -3.68$, $P = 0.003$] and 1 vs. 6 [$t(19) = -3.79$, $P = 0.002$]; the other differences were NS (P's ≥ 0.30). Bayesian repeated measures ANOVA revealed moderate evidence against the inclusion of feature ($BF_{incl} = 0.22$) and the interaction effect ($BF_{incl} = 0.15$) in the model, and strong evidence for the inclusion of load ($BF_{incl} = 29.78$) in the model. There was moderate evidence for the difference between 1 vs. 2 ($BF_{10} = 4.80$) and 1 vs. 6 ($BF_{10} = 29.58$) and strong evidence for the difference between 1 vs. 4 ($BF_{10} = 44.75$); there was moderate evidence against the difference between 4 vs. 6 ($BF_{10} = 0.17$), suggesting a plateau beyond ~4. Evidence for the difference between 2 vs. 4 ($BF_{10} = 1.80$) and 2 vs. 6 ($BF_{10} = 2.18$) was weak.

For the left ROI, the main effect of load was significant, [$F(1.97,37.36) = 4.75$, $P = 0.015$]. The main effect of feature [$F(1,19) = 1.37$, $P = 0.26$] and the interaction effect [$F(3,57) = 0.42$, $P = 0.74$] were not statistically significant. Post-hoc comparisons (Bonferroni corrected) revealed a significant difference between loads 1 vs. 2 [$t(19) = 2.79$, $P = 0.043$] and 1 vs. 4 [$t(19) = 3.58$, $P = 0.004$]; the other differences were not statistically significant (P's > 0.12). Bayesian repeated measures ANOVA revealed moderate evidence against the inclusion of feature ($BF_{incl} = 0.29$) and the interaction effect ($BF_{incl} = 0.11$) in the model, and moderate evidence for the inclusion of load ($BF_{incl} = 4.79$) in the model. There was moderate evidence for the difference between 1 vs. 2 ($BF_{10} = 22.98$) and 1 vs. 4 ($BF_{10} = 9.58$), and moderate evidence against the difference between 2 vs. 4 ($BF_{10} = 0.25$) and 2 vs. 6 ($BF_{10} = 0.19$), suggesting a plateau beyond ~2. Evidence for the difference between 1 vs. 6 ($BF_{10} = 2.36$) and 4 vs. 6 ($BF_{10} = 0.79$) was weak.

Pooling colored square data from all 40 participants across experiments 1 and 2 together allowed us to conduct a high-powered analysis to determine whether the two ROIs exhibited the monotonic increase up to 4 followed by a plateau, as predicted if there is a limited pointer capacity of ~3 (Fig. 4). For the right ROI, the Bayesian paired-sample t-test revealed moderate evidence for differences between loads 1 vs. 2 ($BF_{10} = 16.07$), 1 vs. 4 ($BF_{10} = 28.00$), 2 vs. 6 ($BF_{10} = 5.50$) and strong evidence for a difference between 1 vs. 6 ($BF_{10} = 134.59$). There was also moderate evidence against a difference between 4 vs. 6 ($BF_{10} = 0.19$). Evidence for the difference between 2 vs. 4 was weak ($BF_{10} = 2.18$) but was still in the direction of a difference. Overall, this suggests a plateau beyond ~ 4 items for the right ROI.

For the left ROI, the Bayesian paired-sample t-test revealed strong evidence for a difference between loads

Fig. 3

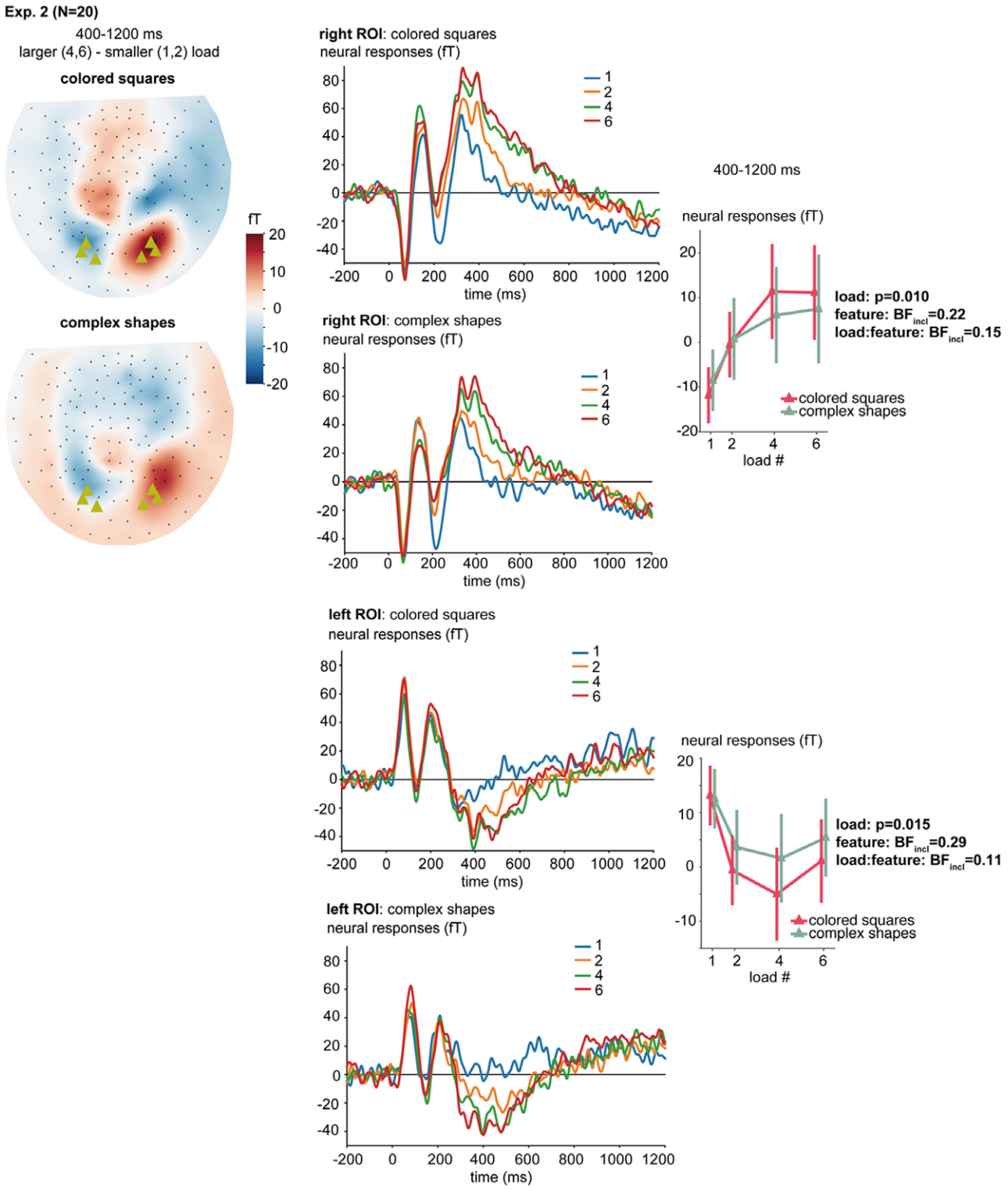

A summary of the MEG results in experiment 2. Error bars stand for standard error. The ROI channels are marked with green triangles. BF, Bayesian factor; MEG, magnetoencephalography; ROI, region of interest.

Fig. 4

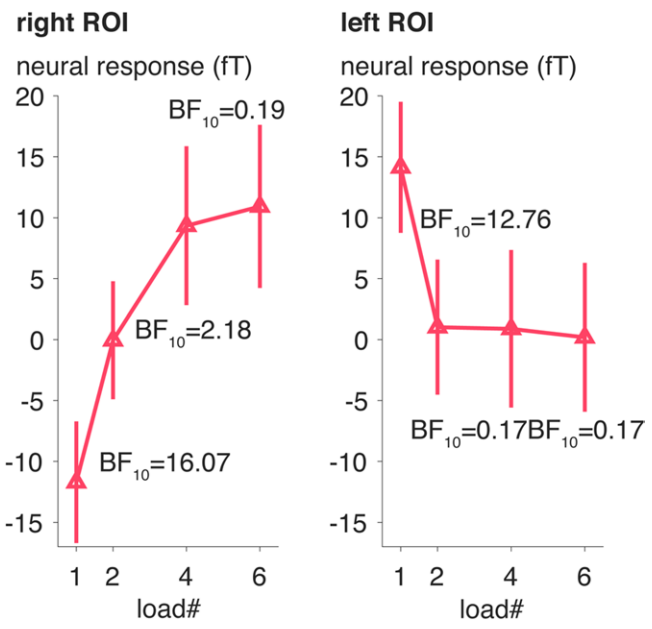

MEG responses during the VWM period (400:1200 ms) for the colored squares in the right and left ROIs, pooled across all 40 participants in experiments 1 and 2. Error bars stand for standard error. BF, Bayesian factor; MEG, magnetoencephalography; ROI, region of interest; VWM, visual working memory.

1 vs. 2 (BF_{10} = 12.76) and moderate evidence for a difference between 1 vs. 6 (BF_{10} = 7.94), and moderate evidence against a difference between loads 2 vs. 4 (BF_{10} = 0.17), 2 vs. 6 (BF_{10} = 0.17), and 4 vs. 6 (BF_{10} = 0.17). Evidence for the difference between 1 vs. 4 was weak (BF_{10} = 2.44) but was still in the direction of a difference. Overall, this suggests a plateau beyond ~2 items for the left ROI.

Discussion

Conclusion

In this study, we observed univariate responses in MEG over right posterior sites (the RPA) that met all three criteria for VWM pointers: load-dependent, capacity-limited, and content-free. This neural response changed monotonically as VWM load increased, reached a plateau at ~4 objects (in line with the classic VWM capacity limit), and was insensitive to the difference in type and number of features bound to each object in the colored square vs. complex shape conditions even though these differences impacted behavioral performance. Given its maxima over right posterior channels, this response is likely to be of posterior parietal origin, in line with previous fMRI effects attributed to VWM pointers [12,24], and consistent with the involvement of the posterior parietal cortex in VWM maintenance in general [41–43]. This awaits to be confirmed by future studies with higher spatial-temporal resolution (e.g. combining MEG with structural MRI and intracranial recordings). Our current study serves as an important complement to prior fMRI studies, in that we confirmed VWM pointer-like responses during the VWM maintenance time window in particular. The right-lateralization of our current effects invites future neuroimaging research on the lateralization of VWM substrates. Intriguingly, this is in line with some neuropsychological reports suggesting that unilateral right posterior parietal lesions are sufficient for an impaired VWM (for a review and nuanced discussions see [44]).

We also found that left posterior channels exhibited a load-dependent, capacity-limited, and content-free effect, but this response plateaued at only ~2 objects. While this different response profile awaits future investigation, it could reflect cognitive effort related to pattern-separating more than one feature of the same type (e.g. when one needs to hold multiple colors in VWM) or mechanisms related to attention allocation [45].

Limitations and future directions

As this is only the first MEG study exploring content-free neural signatures in VWM, future studies are certainly needed in order to address some limitations of the current work. First, in our current study, the number of trials per condition was lower than previous MEG studies on VWM load (as noted in the 'Magnetoencephalography (MEG) results' section). It is yet unknown how many trials are sufficient to detect differences across VWM load conditions for the posterior activities in MEG [46]. We only obtained weak evidence for the difference between two and four objects in the right posterior ROI (BF_{10} = 2.18), and more evidence is needed to confirm the existence of this difference. Second, in our current study, the number of pointers may covary with, for example, the number of locations in or the luminance of the memorandum display [10], which could be controlled for in future studies. Furthermore, it would be interesting to examine whether RPA could predict individual differences in VWM capacity [29,30].

Acknowledgements

The authors thank Marco Chia-Ho Lai and Ciaran Stone for the discussions on MEG data analysis.

This work is supported by NSF #1749407 (to E.L.).

Conceptualization, data curation, investigation, formal analysis, methodology, software, visualization, writing – original draft, and writing – review and editing: X.Y. Conceptualization, funding acquisition, methodology, supervision, and writing – review and editing: E.L.

Our raw, processed data and analysis scripts are openly shared on the Open Science Framework (https://osf.io/nmsj5/).

Conflicts of interest

There are no conflicts of interest.

References

1 Cowan N. The magical number 4 in short-term memory: a reconsideration of mental storage capacity. *Behav Brain Sci* 2001; **24**:87–114; discussion 114.
2 Luck SJ, Vogel EK. The capacity of visual working memory for features and conjunctions. *Nature* 1997; **390**:279–281.
3 Bays PM, Schneegans S, Ma WJ, Brady TF. Representation and computation in working memory. *Nat Hum Behav* 2024; **8**:1016–1034.
4 Fukuda K, Awh E, Vogel EK. Discrete capacity limits in visual working memory. *Curr Opin Neurobiol* 2010; **20**:177–182.
5 Ma WJ, Husain M, Bays PM. Changing concepts of working memory. *Nat Neurosci* 2014; **17**:347–356.
6 Zhang W, Luck SJ. Discrete fixed-resolution representations in visual working memory. *Nature* 2008; **453**:233–235.
7 Xu Y. Reevaluating the sensory account of visual working memory storage. *Trends Cogn Sci* 2017; **21**:794–815.
8 Ngiam WXQ. Mapping visual working memory models to a theoretical framework. *Psychon Bull Rev* 2024; **31**:442–459.
9 Swan G, Wyble B. The binding pool: a model of shared neural resources for distinct items in visual working memory. *Atten Percept Psychophys* 2014; **76**:2136–2157.
10 Thyer W, Adam KCS, Diaz GK, Velázquez Sánchez IN, Vogel EK, Awh E. Storage in visual working memory recruits a content-independent pointer system. *Psychol Sci* 2022; **33**:1680–1694.
11 Yu X, Lau E. The binding problem 2.0: beyond perceptual features. *Cogn Sci* 2023; **47**:e13244.
12 Xu Y, Chun MM. Dissociable neural mechanisms supporting visual short-term memory for objects. *Nature* 2006; **440**:91–95.
13 Balaban H, Smith KA, Tenenbaum JB, Ullman T. Electrophysiology reveals that intuitive physics guides visual tracking and working memory. *Open Mind* 2023; **8**:1425–1446.
14 Balaban H, Drew T, Luria R. Dissociable online integration processes in visual working memory. *Cereb Cortex* 2023; **33**:11420–11430.
15 Pylyshyn ZW. The role of location indexes in spatial perception. *Cognition* 1989; **32**:65–97.
16 Zhou K, Luo H, Zhou T, Zhuo Y, Chen L. Topological change disturbs object continuity in attentive tracking. *Proc Natl Acad Sci USA* 2010; **107**:21920–21924.
17 Park B, B. Walther D, Fukuda K. Dynamic representations in visual working memory. *J Vis* 2020; **20**:900.
18 Bowman H, Wyble B. The simultaneous type, serial token model of temporal attention and working memory. *Psychol Rev* 2007; **114**:38–70.
19 Hedayati S, O'Donnell RE, Wyble B. A model of working memory for latent representations. *Nat Hum Behav* 2022; **6**:709–719.
20 Green EJ, Quilty-Dunn J. What is an object file? *Br J Philos Sci* 2021; **72**:665–699.
21 Wang B, Cao X, Theeuwes J, Olivers CNL, Wang Z. Separate capacities for storing different features in visual working memory. *J Exp Psychol Learn Mem Cogn* 2017; **43**:226–236.
22 Wilson KE, Adamo M, Barense MD, Ferber S. To bind or not to bind: addressing the question of object representation in visual short-term memory. *J Vis* 2012; **12**:14–14.
23 Balaban H, Drew T, Luria R. Neural evidence for an object-based pointer system underlying working memory. *Cortex* 2019; **119**:362–372.
24 Naughtin CK, Mattingley JB, Dux PE. Distributed and overlapping neural substrates for object individuation and identification in visual short-term memory. *Cereb Cortex* 2016; **26**:566–575.
25 Mitchell DJ, Cusack R. The temporal evolution of electromagnetic markers sensitive to the capacity limits of visual short-term memory. *Front Hum Neurosci* 2011; **5**:1–20.
26 Robitaille N, Grimault S, Jolicœur P. Bilateral parietal and contralateral responses during maintenance of unilaterally encoded objects in visual short-term memory: evidence from magnetoencephalography. *Psychophysiology* 2009; **46**:1090–1099.
27 Robitaille N, Marois R, Todd J, Grimault S, Cheyne D, Jolicœur P. Distinguishing between lateralized and nonlateralized brain activity associated with visual short-term memory: fMRI, MEG, and EEG evidence from the same observers. *Neuroimage* 2010; **53**:1334–1345.
28 Adam KCS, Vogel EK, Awh E. Multivariate analysis reveals a generalizable human electrophysiological signature of working memory load. *Psychophysiology* 2020; **57**:1–17.
29 Vogel EK, Machizawa MG. Neural activity predicts individual differences in visual working memory capacity. *Nature* 2004; **428**:748–751.
30 Luria R, Balaban H, Awh E, Vogel EK. The contralateral delay activity as a neural measure of visual working memory. *Neurosci Biobehav Rev* 2016; **62**:100–108.
31 Arend AM, Zimmer HD. What does ipsilateral delay activity reflect? Inferences from slow potentials in a lateralized visual working memory task. *J Cogn Neurosci* 2011; **23**:4048–4056.
32 Mccollough AW, Machizawa MG, Vogel EK. Electrophysiological measures of maintaining representations in visual working memory. *Cortex* 2007; **43**:77–94.
33 Becke A, Müller N, Vellage A, Schoenfeld MA, Hopf JM. Neural sources of visual working memory maintenance in human parietal and ventral extrastriate visual cortex. *Neuroimage* 2015; **110**:78–86.
34 Brainard DH. The psychophysics toolbox. *Spat Vis* 1997; **10**:433–436.
35 Kleiner M, Brainard D, Pelli D, Ingling A, Murray R, Broussard C. ECVP '07 abstracts. *Perception* 2007; **36**(1_suppl):1–235.
36 Rouder JN, Morey RD, Morey CC, Cowan N. How to measure working memory capacity in the change detection paradigm. *Psychon Bull Rev* 2011; **18**:324–330.
37 Gramfort A, Luessi M, Larson E, Engemann DA, Strohmeier D, Brodbeck C, *et al*. MEG and EEG data analysis with MNE-Python. *Front Neurosci* 2013; **7**:1–13.
38 Taulu S, Simola J. Spatiotemporal signal space separation method for rejecting nearby interference in MEG measurements. *Phys Med Biol* 2006; **51**:1759–1768.
39 JASP Team. JASP 0.18.1. 2023.
40 van Doorn J, van den Bergh D, Böhm U, Dablander F, Derks K, Draws T, *et al*. The JASP guidelines for conducting and reporting a Bayesian analysis. *Psychon Bull Rev* 2021; **28**:813–826.
41 Xu Y. Parietal-driven visual working memory representation in occipito-temporal cortex. *Curr Biol* 2023; **33**:4516–4523.e5.
42 Marois R, Todd JJ. Capacity limit of visual short-term memory in human posterior parietal cortex. *Nature* 2004; **428**:751–754.
43 Matsuyoshi D, Ikeda T, Sawamoto N, Kakigi R, Fukuyama H, Osaka N. Task-irrelevant memory load induces inattentional blindness without temporo-parietal suppression. *Neuropsychologia* 2010; **48**:3094–3101.
44 Olson IR, Berryhill M. Some surprising findings on the involvement of the parietal lobe in human memory. *Neurobiol Learn Mem* 2009; **91**:155–165.
45 Todd JJ, Marois R. Posterior parietal cortex activity predicts individual differences in visual short-term memory capacity. *Cogn Affect Behav Neurosci* 2005; **5**:144–155.
46 Ngiam WXQ, Adam KCS, Quirk C, Vogel EK, Awh E. Estimating the statistical power to detect set-size effects in contralateral delay activity. *Psychophysiology* 2021; **58**:1–10.